Vertical vibrations of a bridge based on the traffic-pavement-bridge coupled system

Yin Xinfeng[1], Liu Yang[*1] and Kong Bo[2]

[1]*School of Civil Engineering and Architecture, Changsha University of Science & Technology, Changsha 410004, Hunan, China*
[2]*Department of Civil and Environmental Engineering, Louisiana State University, Baton Rouge, Louisiana, 70803, USA*

Abstract.   When studying the vibration of a suspension bridge based on the traffic-bridge coupled system, most researchers ignored the contribution of the pavement response. For example, the pavement was simplified as a rigid base and the deformation of pavement was ignored. However, the action of deck pavement on the vibration of vehicles or bridges should not be neglected. This study is mainly focused on establishing a new methodology fully considering the effects of bridge deck pavement, probabilistic traffic flows, and varied road roughness conditions. The bridge deck pavement was modeled as a boundless Euler-Bernoulli beam supported on the Kelvin model; the typical traffic flows were simulated by the improved Cellular Automaton (CA) traffic flow model; and the traffic-pavement-bridge coupled equations were established by combining the equations of motion of the vehicles, pavement, and bridge using the displacement and interaction force relationship at the contact locations. The numerical studies show that the proposed method can more rationally simulate the effect of the pavement on the vibrations of bridge and vehicles.

Keywords: traffic-pavement-bridge coupled system; bridge; vehicle; road surface

1. Introduction

The studies on the bridge vibration under moving vehicles have been extensively conducted and achieved great success during the recent decades. The dynamic performance of bridges is affected by many factors, such as the vehicle type, vehicle speed, and road surface condition. In the literature, some vehicle-bridge interaction models have been proposed. For example, the vehicles have been simulated as a single degree-of-freedom (DOF) system, two-DOF system (Fryba 1974, Wang *et al.*1992, Green and Cebon 1997), or a more complex seven-DOF system (Deng and Cai 2010, Deng and Cai 2011, Zhang and Cai 2012). The bridges have been modeled as simply-support beams (Law and Zhu 2005) or multi-span continuous beams (Yin *et al.* 2010, Yang *et al.* 2013). However, the effects of the bridge deck pavement on the vibration of vehicles or bridge structures were neglected by most researchers.

Recently, the stochastic characteristics of traffic flows were studied and significant effect was found on the dynamic performance of long-span bridges (Chen and Wu 2010, Zhou and Chen 2014, Yin *et al.* 2016). However, the contribution of pavement response was still not considered in these studies for vehicle-bridge coupled vibration. For example, the pavement was simplified as a rigid base and the deformation of pavement was ignored (Chen and Wu

2010, Yin *et al.* 2011, Yang *et al.* 2013). In reality, when a vehicle travelling on the pavement, the wheel forces are generated and applied to the pavement, which in turn induces an increment in pavement response and affects the amount of distress produced by the vehicle. In most existing studies, the vehicle-pavement coupled vibrations were focused on studies of road layers or pavement design. Markow *et al.* (1988) stated that the pavement dynamic loads resulting from moving vehicles is of significance in pavement design. To evaluate the dynamic performance of pavements under moving vehicles, Mamlouk (1997) provided an overview on the research related to the pavement and vehicle dynamics and their interactions. Andersen *et al.* (2001) dealt with the problem of loads moving uniformly along an infinite Euler beam supported on a Kelvin foundation by the finite element method. Kim and McCullough (2003) investigated the dynamic displacements and stress responses of an infinite thin plate on a viscous Winkler foundation subjected to moving tandem-axle loads. Kuo *et al.* (2011) and Cao *et al.* (2011) discussed the dynamic responses of the pavement under moving vehicles. The dynamic response of Euler-Bernoulli beams resting on foundations and subjected to moving loads has been extensively studied, and a number of literatures have been published in recent years (Andersen *et al.* 2001, Cao *et al.* 2011, Heider *et al.* 2014). However, those all studies mention above, the researchers were focused on studies of road layers or pavement design but not on the contribution of pavement on the bridge vibration under moving vehicles.

This study is mainly focused on establishing a new

---

*Corresponding author, Professor
 E-mail: yinxinfeng@163.com

methodology fully considering the effects of bridge deck pavement, probabilistic traffic flows, and varied road roughness conditions. The bridge deck pavement was modeled as the Euler-Bernoulli beam supported on the Kelvin model; the typical traffic flows were simulated by the improved Cellular Automaton (CA) traffic flow model; two vehicle models, i.e., a eighteen DOFs vehicle model and a single vehicle model, respectively, were used to simulate all vehicles in the traffic flows to be computationally efficient; and the traffic-pavement-bridge coupled equations were established by combining the equations of motion of both the vehicles, pavement, and bridge using the displacement and interaction force relationship at the contact locations.

2. Method of traffic-pavement-bridge coupled system

2.1 Traffic flow simulation

The CA traffic model can capture the basic features of probabilistic traffic flows by adopting the realistic traffic rules such as the car-following, lane-changing, and speed limits. One of the most important CA models is the Nagel-Schreckenberg (NaSch) model (Nagel and Schreckenberg 1992). Though the NaSch model is simple, it can describe some real traffic phenomena, such as the phase transition. In recent years, the CA-based traffic flow simulation model was introduced to study the vibration of bridges under traffic flows and satisfactory results were obtained (Chen and Wu 2010). All previously adopted CA models, however, did not take into account of the influence from the next-nearest neighbor vehicle, which cannot be ignored because of its influence on the real traffic (Kong *et al.* 2006). In this paper, a CA model that can consider the influence of the next-nearest neighbor vehicle, which was proposed by Kong *et al.* (2006), was used to simulate the traffic flow.

In the CA model, the influence of the vehicle ahead was considered by using the following equation (Kong *et al.* 2006)

$$\ddot{x}_n(t+T) = \lambda(\dot{x}_{n+1} - \dot{x}_n) \tag{1}$$

where T is a response time lag; λ is the sensitivity coefficient; $\ddot{x}_n$ is the acceleration of the vehicle; and $\dot{x}_n$ is the velocity of the vehicle . The model shows that the response of the following vehicle is in direct proportion to the stimulus received from the leading vehicle. Considering the influence of the next-nearest neighbor vehicle, Eq. (1) can be expressed as

$$\ddot{x}_n = \lambda_1(\dot{x}_{n+1} - \dot{x}_n)_{t-T_1} + \lambda_2(\dot{x}_{n+2} - \dot{x}_n)_{t-T_2} \tag{2}$$

where T_1 is a response time lag of the nearest neighbor vehicle ahead; T_2 is a response time lag of the next-nearest neighbor vehicle ahead; and λ_1 and λ_2 are the sensitivity coefficients corresponding to T_1 and T_2, respectively, and both of them are confined from 0 to 1 and $\lambda_1 > \lambda_2$. In this way, the rules for the acceleration/deceleration of vehicles

can be adjusted in the NaSch model by using Eq. (2). Thus, the two-lane CA model considering the influence of next-nearest neighbor vehicle was established for the tested highway bridge in the following discussion.

2.2 Equations of motion for vehicles in the traffic

In the present study, in order to simplify the vehicular models in traffic flows (Chen and Cai 2007), all vehicles are classified as three types: heavy multi-axle trucks, light trucks and buses, and sedan car. Only heavy trucks are modeled with three dimensional vehicle models, while the light trucks and sedan cars are simulated with the single DOF vehicle model to be computationally efficient. The three dimensional vehicle models and single DOF vehicle models are shown in Fig. 1 and Fig. 2, respectively.

The DOFs of three dimensional vehicle model and single DOF vehicle model include the longitudinal displacements (x_t), vertical displacements (z_t), lateral displacements (y_t), pitching rotations (θ_t), roll displacements (ϕ_t), and yawing angle (φ_t) of the vehicle body, and the longitudinal displacement $(x_a^1, x_a^2, x_a^3, \text{ and } x_a^4)$, vertical displacements $(z_a^1, z_a^2, z_a^3, \text{ and } z_a^4)$ and lateral displacements $(y_a^1, y_a^2, y_a^3, \text{ and } y_a^4)$ of the vehicle's first to second axles, respectively.

(a) Elevation view

(b) Cross-section view

Fig. 1 The three dimensional vehicle model

(a) Elevation view　　(b) Cross-section view
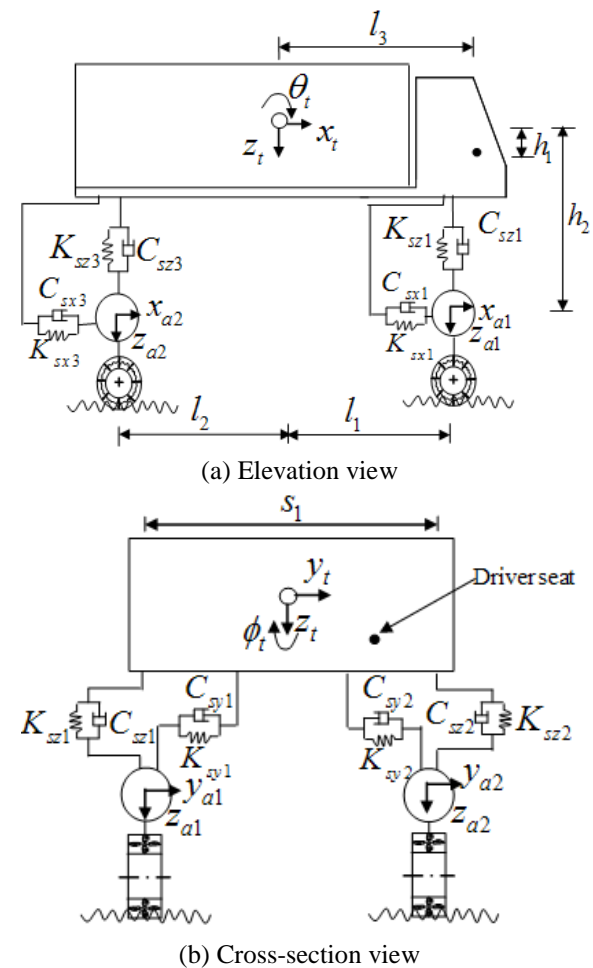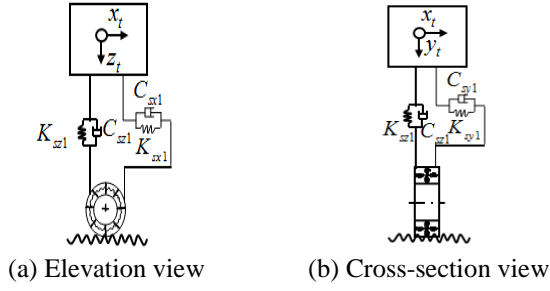
Fig. 2 The single DOF vehicle model

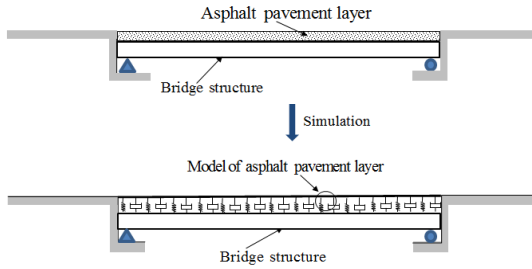Fig. 3 The pavement model

The equation of motion of the vehicle model can be written as

$$[M_v]\{\ddot{U}_v\}+[C_v]\{\dot{U}_v\}+[K_v]\{U_v\}=\{F_G\}+\{F_{v\text{-}p}\} \quad (3)$$

Where $[M_v]$, $[C_v]$, and $[K_v]$=the mass, damping, and stiffness matrices of the vehicle, respectively; $\{U_v\}$=the vector including the displacements of the vehicle; $\{F_G\}$=gravity force vector of the vehicle; and $\{F_{v\text{-}p}\}$=vector of the wheel-pavement contact forces acting on the vehicle.

2.3 Equations of motion for pavement and bridge model

Based on the pavement studies (Mamlouk 1997, Andersen *et al*. 2001, Cao *et al*. 2011), the pavement can be modeled as an Euler-Bernoulli beam supported on the Kelvin model, as shown in Fig. 3.

The equation of motion of a pavement model can be writen as

$$E_p I_p y_p''''+m_p \ddot{y}_p+c_p \dot{y}_p =(F_G+F_{v\text{-}b})\delta(x-vt)-$$
$$K_k(y_p-y_b)-C_k(\dot{y}_p-\dot{y}_b) \quad (4)$$

or

$$[M_P]\{\ddot{U}_P\}+[C_P]\{\dot{U}_P\}+[K_P]\{U_P\}=$$
$$\{F_{p\text{-}v}\}-\{F_{P\text{-}b}\} \quad (5)$$

Where $[M_p]$, $[C_p]$, and $[K_p]$ are the mass, damping, and stiffness matrices of the pavement, respectively; $\{U_p\}$ is the displacement vector for all DOFs of the pavement; $\{\dot{U}_p\}$ and $\{\ddot{U}_p\}$ are the first and second derivative of $\{U_p\}$ with respect to time, respectively; and $\{F_{p\text{-}v}\}$ is a vector containing all external forces acting on the pavement;

$\{F_{p\text{-}b}\}$ is a vector containing interaction forces between bridge and pavement.

The equation of motion of a bridge structural model can be written as

$$E_b I_b y_b''''+m_b \ddot{y}_b+c_b \dot{y}_b = K_k(y_p-y_b)+C_k(\dot{y}_p-\dot{y}_b) \quad (6)$$

or

$$[M_b]\{\ddot{U}_b\}+[C_b]\{\dot{U}_b\}+[K_b]\{U_b\}=\{F_{b\text{-}p}\} \quad (7)$$

where $[M_b]$, $[C_b]$, and $[K_b]$ are the mass, damping, and stiffness matrices of the bridge, respectively; $\{U_b\}$ is the displacement vector for all DOFs of the bridge; $\{\dot{U}_b\}$ and $\{\ddot{U}_b\}$ are the first and second derivative of $\{U_b\}$ with respect to time, respectively; and $\{F_{b\text{-}p}\}$ is a vector containing interaction forces between bridge and pavement.

2.4 Assembling the vehicle-pavement-bridge coupled system

Vehicles traveling on the pavement are connected to the pavement via patch contacts. The interaction forces acting on the pavement $\{F_{p-v}\}$ and the interaction forces acting on the vehicles $\{F_{v-p}\}$ are actually a pair of action and reaction forces existing at the patch contacts. In terms of finite element modeling, these interaction forces may not be applied right at any nodes. Therefore, the interaction forces need to be transformed into equivalent nodal forces $\{F_b^{eq}\}$ in the finite element analysis. This can be done using the virtual work principle, which states that the work done by the equivalent nodal forces and the actual force should be equal. Thus, it can be expressed as

$$\{y_{p\_nodal}\}^T \{F^{eq}\} = y_{px\_contact} \cdot F \quad (8)$$

where $\{y_{p\_nodal}\}$ is the displacement vector for all the nodes of the element in contact; $y_{px\_contact}$ is the displacement of the element bearing the tire spring load at the contact position x; $\{F^{eq}\}$ is the equivalent force vector applied at all the nodes of the element in contact; and F is the real force acting at the patch contact.

The $y_{px\_contact}$ can be expressed using the displacement at each node of the element as

$$y_{px\_contact} = [N_e]\{y_{p\_nodal}\} \quad (9)$$

where $[N_e]$ is the relationship function of the element in contact. From Eqs. (8) and (9), the relationship between the equivalent nodal forces and the interaction force acting on the element in contact is expressed as

$$\{F^{eq}\}=[N_e]^T \cdot F \quad (10)$$

To be consistent with the size of the force vector $\{F_p^{eq}\}$ in the analysis of the full pavement, Eq. (10) can be expanded to a full force vector form as

$$\{F_p{}^{eq}\} = [N_p]^T \cdot F \qquad (11)$$

where $\{F_p{}^{eq}\}$ is a vector with the number of elements equal to the total number of DOFs of the pavement. It should be noted that, for two interaction forces acting upon different elements of the same pavement, the relationship function of the pavement $[N_p]$ for the two forces would be different though the element relationship function $[N_e]$ may be the same, because the corresponding DOFs of the non-zero terms in the two force vectors are different.

In a pavement-vehicle system, the relationship among the vertical displacement of vehicle body $y_v{}^i$, pavement deflection at the contact position $y^i_{px\_contact}$, the radial deformation of *ith* tire spring $U_{tyx}{}^i$ at the position *x*, and road surface profile $r(x)^i$, can be rewritten as

$$U_{tyx}{}^i = \{y_v{}^i - [-r(x)^i] - y^i_{px\_contact}\}/\cos\theta$$
$$y_v{}^i = y_a{}^j \pm (s_j/2)\phi_a{}^j + \Delta^i - R(1-\cos\theta), \quad j=1,2 \qquad (12)$$

The first derivative of Eq. (12) can then be obtained as

$$\dot{U}_{tyx}{}^i = (\dot{y}_v{}^i + \dot{r}(x)^i - \dot{y}^i_{px\_contact})/\cos\theta \qquad (13)$$

where $\dot{y}_v{}^i$ is the velocity of the vehicle body in the vertical direction; $\dot{r}(x)^i = \dfrac{dr(x)^i}{dx}\dfrac{dx}{dt} = \dfrac{dr(x)^i}{dx}v(t)$, where $v(t)$ is the vehicle traveling velocity; and $\dot{y}^i_{px\_contact}$, according to the definition of the relationship function of the pavement in Eq. (9), can be expressed as

$$y^i_{px\_contact} = [N_e]\cdot\{y^i_{p\_nodal}\} = [N_p]\cdot\{y_p\} \qquad (14)$$

The interaction force acting on the *i*th tire can be obtained as

$$F_{v-p}{}^i = -F_{ty}{}^i - F_{dty}{}^i$$
$$= -\int_{x^i-l_{ty}/2}^{x^i+l_{ty}/2} k_{ty}{}^i\left(y_v{}^i + r(x)^i - [N_p{}^i]\{y_p\}\right)dx - \int_{x^i-l_{ty}/2}^{x^i+l_{ty}/2} c_{ty}{}^i\left(\dot{y}_v{}^i - \frac{d[N_p{}^i]}{dx}v^i(t)\{y_p\} - [N_p{}^i]\{\dot{y}_p\} + \frac{dr(x)^i}{dx}v^i(t)\right)dx \qquad (15)$$

Compared the length of l_{ty} with the total length of the bridge, the l_{ty} is small. Therefore, the value of y_p and y_v can be assumed as a constant in the length range form $x^i - l_{ty}/2$ to $x^i + l_{ty}/2$. Eq. (15) can be further written as

$$F_{v-p}{}^i = -\int_{x^i-l_{ty}/2}^{x^i+l_{ty}/2} k_{ty}{}^i\left(y_v{}^i + r(x)^i - [N_p{}^i]\{y_p\}\right)dx - \int_{x^i-l_{ty}/2}^{x^i+l_{ty}/2} c_{ty}{}^i\left(\dot{y}_v{}^i - \frac{d[N_p{}^i]}{dx}v^i(x)\{y_p\} - [N_p{}^i]\{\dot{y}_p\} + \frac{dr(x)^i}{dx}v^i(t)\right)dx$$
$$= -\int_{x^i-l_{ty}/2}^{x^i+l_{ty}/2} k_{ty}{}^i dx y_v{}^i - \int_{x^i-l_{ty}/2}^{x^i+l_{ty}/2} k_{ty}{}^i r(x)dx + \int_{x^i-l_{ty}/2}^{x^i+l_{ty}/2} k_{ty}{}^i [N_p{}^i]dx\{y_p\} - \int_{x^i-l_{ty}/2}^{x^i+l_{ty}/2} c_{ty}{}^i dx \dot{y}_v{}^i + \int_{x^i-l_{ty}/2}^{x^i+l_{ty}/2} c_{ty}{}^i \frac{d[N_p{}^i]}{dx}v^i(t)dx\{y_p\} \qquad (16)$$
$$+ \int_{x^i-l_{ty}/2}^{x^i+l_{ty}/2} c_{ty}{}^i[N_p{}^i]dx\{\dot{y}_p\} - \int_{x^i-l_{ty}/2}^{x^i+l_{ty}/2} c_{ty}{}^i \frac{dr(x)^i}{dx}v^i(t)dx$$

where $[N_p{}^i]$ is the relationship function of the bridge for an interaction force between the *i*th tire and the pavement.

The *N* interaction forces can be expressed in a vector form as

$$\{F_{v-p}{}^N\} = \{F_{v-p}{}^1 \quad F_{v-p}{}^2 \cdots F_{v-p}{}^N\}^T$$
$$= -[K_{v-v}{}^N]\{y_v\} - \{F_{v-r}\} + [K_{v-p}]\{y_p\} - [C_{v-v}{}^N]\{\dot{y}_v\} + [K_{v-cp}]\{y_p\} + [C_{v-p}]\{\dot{y}_p\} - \{F_{v-cr}\} \qquad (17)$$

where $[K_{v-v}{}^N]$ and $[C_{v-v}{}^N]$ are the stiffness, and damping matrices for *N* tires, respectively; and $[K_{v-p}]$, $\{F_{v-r}\}$, $[K_{v-cp}]$, $[C_{v-p}]$, and $\{F_{v-cr}\}$ are defined, respectively, as

$$[K_{v-v}{}^N] = \left[\int_{x^1-l_{ty}/2}^{x^1+l_{ty}/2} k_{ty}{}^1 dx \quad \int_{x^2-l_{ty}/2}^{x^2+l_{ty}/2} k_{ty}{}^2 dx \cdots \int_{x^N-l_{ty}/2}^{x^N+l_{ty}/2} k_{ty}{}^N dx\right]$$

$$[C_{v-v}{}^N] = \left[\int_{x^1-l_{ty}/2}^{x^1+l_{ty}/2} c_{ty}{}^1 dx \quad \int_{x^2-l_{ty}/2}^{x^2+l_{ty}/2} c_{ty}{}^2 dx \cdots \int_{x^N-l_{ty}/2}^{x^N+l_{ty}/2} c_{ty}{}^N dx\right]$$

$$[K_{v-p}] = [K_{v-v}{}^N]\cdot\left[\int_{x^1-l_{ty}/2}^{x^1+l_{ty}/2} [N_p{}^1]^T dx \right.$$
$$\left. \int_{x^2-l_{ty}/2}^{x^2+l_{ty}/2} [N_p{}^2]^T dx \cdots \int_{x^N-l_{ty}/2}^{x^N+l_{ty}/2} [N_p{}^N]^T dx\right]^T$$

$$\{F_{v-r}\} = [K_{v-v}{}^N]\cdot\left[\int_{x^1-l_{ty}/2}^{x^1+l_{ty}/2} r(x)^1 dx \quad \int_{x^2-l_{ty}/2}^{x^2+l_{ty}/2} r(x)^2 dx \cdots \int_{x^N-l_{ty}/2}^{x^N+l_{ty}/2} r(x)^N dx\right]^T$$

$$[K_{v-cp}] = [C_{v-v}{}^N]\left[\int_{x^1-l_{ty}/2}^{x^1+l_{ty}/2} \frac{d[N_p{}^1]^T}{dx}v^1(t)dx \quad \int_{x^2-l_{ty}/2}^{x^2+l_{ty}/2} \frac{d[N_p{}^2]^T}{dx}v^2(t)dx \cdots \int_{x^N-l_{ty}/2}^{x^N+l_{ty}/2} \frac{d[N_p{}^N]^T}{dx}v^N(t)dx\right]^T;$$

$$[C_{v-p}] = [C_{v-v}{}^N]\cdot\left[\int_{x^1-l_{ty}/2}^{x^1+l_{ty}/2} [N_p{}^1]^T dx \quad \int_{x^2-l_{ty}/2}^{x^2+l_{ty}/2} [N_p{}^2]^T dx \cdots \int_{x^N-l_{ty}/2}^{x^N+l_{ty}/2} [N_p{}^N]^T dx\right]^T$$

$$\{F_{v-cr}\} = [C_{v-v}{}^N]\cdot\left[\int_{x^1-l_{ty}/2}^{x^1+l_{ty}/2} \frac{dr(x)^1}{dx}v^1(t)dx \quad \int_{x^2-l_{ty}/2}^{x^2+l_{ty}/2} \frac{dr(x)^2}{dx}v^2(t)dx \cdots \int_{x^N-l_{ty}/2}^{x^N+l_{ty}/2} \frac{dr(x)^N}{dx}v^N(t)dx\right]^T$$

As discussed earlier, the interaction forces acting on the pavement, $\{F_{p-v}\}$, are the reaction forces of that acting on the vehicles, $\{F_{v-p}\}$. Therefore, the following relationship holds

$$\{F_{p-v}\} = -\{F_{v-p}\} \qquad (18)$$

Substituting Eqs. (16) and (18) into Eq. (11), the transformed equivalent nodal forces due to the *N* interaction forces can be obtained as

$$\{F_p{}^{eq}\} = \sum_{i=1}^{N}[N_p{}^i]^T\cdot(-F_{v-p}{}^i)$$
$$= \sum_{i=1}^{N}[N_p{}^i]^T\cdot\left[\begin{array}{l}\int_{x^i-l_{ty}/2}^{x^i+l_{ty}/2} k_{ty}{}^i dx y_v{}^i + \int_{x^i-l_{ty}/2}^{x^i+l_{ty}/2} k_{ty}{}^i r(x)^i dx - \int_{x^i-l_{ty}/2}^{x^i+l_{ty}/2} k_{ty}{}^i [N_p{}^i]dx\{y_p\} + \int_{x^i-l_{ty}/2}^{x^i+l_{ty}/2} c_{ty}{}^i dx \dot{y}_v{}^i \\ -\int_{x^i-l_{ty}/2}^{x^i+l_{ty}/2} c_{ty}{}^i \frac{d[N_p{}^i]}{dx}v^i(t)dx\{y_p\} - \int_{x^i-l_{ty}/2}^{x^i+l_{ty}/2} c_{ty}{}^i [N_p{}^i]dx\{\dot{y}_p\} + \int_{x^i-l_{ty}/2}^{x^i+l_{ty}/2} c_{ty}{}^i \frac{dr(x)^i}{dx}v^i(t)dx\end{array}\right] \qquad (19)$$
$$= [K_{p-v}]\{y_v\} + \{F_{p-r}\} - [K_{p-vp}]\{y_p\} + [C_{p-v}]\{\dot{y}_v\} - [K_{p-cp}]\{y_p\} - [C_{p-p}]\{\dot{y}_p\} + \{F_{p-cr}\}$$

where $[K_{p-v}]$, $[K_{p-vp}]$, $\{F_{p-r}\}$, $[C_{p-v}]$, $[K_{p-cp}]$, $[C_{p-p}]$, and $\{F_{p-cr}\}$ are defined as

$$[K_{p-v}] = \left\{[N_p{}^1]^T\cdot\int_{x^1-l_{ty}/2}^{x^1+l_{ty}/2} k_{ty}{}^1 dx \quad [N_p{}^2]^T\cdot\int_{x^2-l_{ty}/2}^{x^2+l_{ty}/2} k_{ty}{}^2 dx \cdots [N_p{}^N]^T\cdot\int_{x^N-l_{ty}/2}^{x^N+l_{ty}/2} k_{ty}{}^N dx\right\};$$

$$[K_{p-vp}] = \sum_{i=1}^{n} [N_p^i]^T \int_{x^i-l_{ty}/2}^{x^i+l_{ty}/2} k_{ty}^i [N_p^i] dx;$$

$$\{F_{p-r}\} = \sum_{i=1}^{n} [N_p^i]^T \int_{x^i-l_{ty}/2}^{x^i+l_{ty}/2} k_{ty}^i r(x)^i dx;$$

$$[C_{p-v}] = \left\{ [N_p^1]^T \int_{x^1-l_{ty}/2}^{x^1+l_{ty}/2} c_{ty}^1 dx \quad [N_p^2]^T \int_{x^2-l_{ty}/2}^{x^2+l_{ty}/2} c_{ty}^2 dx \cdots [N_p^N]^T \int_{x^N-l_{ty}/2}^{x^N+l_{ty}/2} k_{ty}^N dx \right\};$$

$$[K_{p-cp}] = \sum_{i=1}^{n} [N_p^i]^T \int_{x^i-l_{ty}/2}^{x^i+l_{ty}/2} c_{ty}^i \frac{d[N_p^i]}{dx} v^i(t) dx;$$

$$[C_{p-p}] = \sum_{i=1}^{n} [N_p^i]^T \int_{x^i-l_{ty}/2}^{x^i+l_{ty}/2} c_{ty}^i [N_p^i] dx;$$

$$\{F_{p-cr}\} = \sum_{i=1}^{n} [N_p^i]^T \int_{x^i-l_{ty}/2}^{x^i+l_{ty}/2} c_{ty}^i \frac{dr(x)^i}{dx} v^i(t) dx;$$

The interaction forces acting on the bridge, $\{F_{p-b}\}$, are the reaction forces of that acting on the pavement, $\{F_{b-p}\}$. Therefore, the following relationship holds

$$\{F_{b-p}\} = K_k \cdot \left(y_{px\_contact}^i - y_{bx\_contact}^i \right) + C_k \cdot \left(\dot{y}_{px\_contact}^i - \dot{y}_{bx\_contact}^i \right)$$

$$= K_k \cdot \left([N_e] \cdot \{y_{p\_nodal}^i\} - [N_e] \cdot \{y_{b\_nodal}^i\} \right) + C_k \cdot \left([N_e] \cdot \{\dot{y}_{p\_nodal}^i\} - [N_e] \cdot \{\dot{y}_{b\_nodal}^i\} \right)$$

$$= K_k \cdot \int_{x^i-l_{ty}/2}^{x^i+l_{ty}/2} ([N_p]\{y_p\}) dx - K_k \cdot \int_{x^i-l_{ty}/2}^{x^i+l_{ty}/2} ([N_b]\{y_b\}) dx + C_k \cdot \int_{x^i-l_{ty}/2}^{x^i+l_{ty}/2} ([N_p]\{\dot{y}_p\}) dx - C_k \int_{x^i-l_{ty}/2}^{x^i+l_{ty}/2} ([N_b]\{\dot{y}_b\}) dx$$

$$= K_k \cdot \int_{x^i-l_{ty}/2}^{x^i+l_{ty}/2} ([N_p]) dx \{y_p\} - K_k \cdot \int_{x^i-l_{ty}/2}^{x^i+l_{ty}/2} ([N_b]) dx \{y_b\} + C_k \cdot \int_{x^i-l_{ty}/2}^{x^i+l_{ty}/2} ([N_p]) dx \{\dot{y}_p\} - C_k \int_{x^i-l_{ty}/2}^{x^i+l_{ty}/2} ([N_b]) dx \{\dot{y}_b\}$$

$$= [K_{b-p}]\{y_p\} - [K_{p-b}]\{y_b\} + [C_{b-p}]\{\dot{y}_p\} - [C_{p-b}]\{\dot{y}_b\}$$

$$[K_{b-p}] = K_k \cdot \int_{x^i-l_{ty}/2}^{x^i+l_{ty}/2} [N_p] dx;$$

$$[K_{p-b}] = K_k \cdot \int_{x^i-l_{ty}/2}^{x^i+l_{ty}/2} [N_b] dx;$$

$$[C_{b-p}] = C_k \cdot \int_{x^i-l_{ty}/2}^{x^i+l_{ty}/2} [N_p] dx;$$

$$[C_{p-b}] = C_k \cdot \int_{x^i-l_{ty}/2}^{x^i+l_{ty}/2} [N_b] dx.$$

Substituting Eq. (17) into Eq. (7)

$$[M_v^N]\{\ddot{y}_v\} + [C_v^N]\{\dot{y}_v\} + [K_v^N]\{y_v\} = F_G^N - [K_{v-v}^N]\{y_v\} +$$

$$[K_{v-p}]\{y_p\} - \{F_{v-r}\} - [C_{v-v}^N]\{\dot{y}_v\} + [K_{v-cp}]\{y_p\} + [C_{v-p}]\{\dot{y}_p\} - \{F_{v-cr}\} \tag{20}$$

Since $\{F_p^{eq}\}$ in Eq. (19) is actually the equivalent force vector of the external force vector $\{F_{p-v}\}$ in Eq. (8), after substituting Eq. (19) into Eq. (8), the following can be obtained

$$[M_p]\{\ddot{y}_p\} + [C_p]\{\dot{y}_p\} + [K_p]\{y_p\} = [K_{p-v}]\{y_v\} - [K_{p-vp}]\{y_p\} + \{F_{p-r}\} + [C_{p-v}]\{\dot{y}_v\} -$$

$$[K_{p-cp}]\{y_p\} - [C_{p-p}]\{\dot{y}_p\} + \{F_{p-cr}\} - [K_{b-p}]\{y_p\} + [K_{p-b}]\{y_b\} - [C_{b-p}]\{\dot{y}_p\} + [C_{p-b}]\{\dot{y}_b\} \tag{21}$$

The equation of motion of a bridge structural model can be written as

$$[M_b]\{\ddot{y}_b\} + [C_b]\{\dot{y}_b\} + [K_b]\{y_b\} = [K_{b-p}]\{y_p\} - [K_{p-b}]\{y_b\} + [C_{b-p}]\{\dot{y}_p\} - [C_{p-b}]\{\dot{y}_b\} \tag{22}$$

2.5 Equations of motion for traffic-pavement-bridge vibration system

In the present study, the heavy truck is modeled with 18 DOFs of the three dimensional vehicle models, and other vehicles are with the single DOF of vehicle model. Using the displacement relationship and the interaction force relationship at the contact patches, the vehicle-bridge coupled system can be established by combining the equations of motion of both the bridge and vehicles. Eqs. (20), (21), and (22) can be combined and rewritten in a matrix form as

$$\begin{bmatrix} M_b & & \\ & M_p & \\ & & M_v^N \end{bmatrix} \begin{Bmatrix} \ddot{Y}_b \\ \ddot{Y}_p \\ \ddot{Y}_v \end{Bmatrix} + \begin{bmatrix} C_b + C_{p-b} & -C_{b-p} & \\ -C_{p-b} & C_p + C_{p-p} & -C_{p-v}^N \\ & -C_{v-p}^N & C_v^N + C_{v-v}^N \end{bmatrix} \begin{Bmatrix} \dot{Y}_b \\ \dot{Y}_p \\ \dot{Y}_v \end{Bmatrix} +$$

$$\begin{bmatrix} K_b + K_{p-b} & -K_{b-p} & \\ -K_{p-b} & K_p + K_{p-vp}^N + K_{p-cp} + K_{b-p} & -K_{p-v}^N \\ & -K_{v-p}^N - K_{v-cp}^N & K_v^N + K_{v-v}^N \end{bmatrix} \begin{Bmatrix} Y_b \\ Y_p \\ Y_v \end{Bmatrix} = \begin{Bmatrix} 0 \\ F_{p-r}^N + F_{p-cr}^N \\ -F_{v-r}^N - F_{v-cr}^N + F_G^N \end{Bmatrix} \tag{23}$$

Where **N** is the number of vehicles traveling on the bridge, $\mathbf{M_v^N}$, $\mathbf{C_v^N}$, and $\mathbf{K_v^N}$ are mass, damping, and stiffness matrices for the vehicle, respectively; $\mathbf{C_{b-vb}^N}$ and $\mathbf{K_{b-vb}^N}$ are damping and stiffness contribution to the bridge structure due to the coupling effects between the N vehicles in the vehicle and the bridge system, respectively; $\mathbf{C_{b-v}^N}$ and $\mathbf{K_{b-v}^N}$ are the coupled stiffness and damping matrices contributing to bridge vibration from the N vehicles in the vehicles, respectively; $\mathbf{C_{v-b}^N}$ and $\mathbf{K_{v-b}^N}$ are the coupled damping and stiffness matrices contributing to the vibration of the N vehicles, respectively; $\mathbf{C_{v-v}^N}$ and $\mathbf{K_{v-v}^N}$ are the coupled damping and stiffness matrices of induced by other vehicles in the vehicles, respectively. Eq. (23) can be solved by the *New-mark* method in the time domain.

2.6 Traffic simulation with different vehicle occupancies

A similar prototype bridge used in the previous study by Chen and Cai (2007) is selected in the present study. The approach roadway at each end of the bridge is assumed to be 1005 m. The speed limit of the highway system is assumed as 135 (km/h), which is converted to the maximum velocity of vehicles in CA model as 5 cell/s. The sensitivity coefficients of the nearest neighbor and next nearest neighbor vehicle are $\lambda_1 = 0.2$ and $\lambda_2 = 0.05$, respectively (Kong *et al.* 2006). The traffic flow simulation results with the CA model usually become stable after a continuous simulation with a period that equals to 10 times the cell numbers of the traffic simulating system (Nagel and Schreckenberg 1992, Chen and Cai 2007), thus similar simulation period is adopted here. For the purpose of comparison, two different vehicle occupancy coefficients ρ are considered (Chen and Wu 2010), i.e., median traffic ($\rho = 0.15$) and busy traffic flow ($\rho = 0.3$). It can be found from Fig. 4 that the *x*-axis and *y*-axis represent the coordinates in the spatial and time

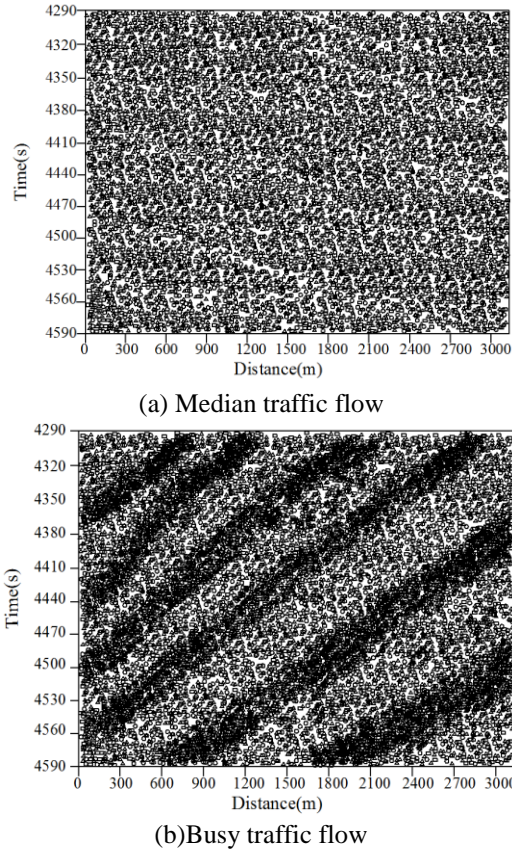(a) Median traffic flow

(b) Busy traffic flow

Fig. 4 Traffic simulation with different vehicle occupancies

Table 1 Statistical property of traffic flow on bridge

Occupancy	Average speed(km/h)	Standard deviation(km/h)
0.15	85.56	24.42
0.30	50.32	39.76

domains, respectively, with each dot on the figures representing a vehicle. With the increase of the traffic occupancy, congestions may be occurred at some locations as indicated by black belts in Fig. 4. It is observed from Table 1 that, with the increase of the vehicle occupancy, the mean speed of the traffic flow decreases while the standard deviation of the vehicle speeds increases.

2.7 Road surface modeling

The road surface condition is an important factor that affects the dynamic responses of both the bridge and vehicles. The road surface profile is usually assumed to be a zero-mean stationary Gaussian random process and can be generated through an inverse Fourier transformation based on a power spectral density (PSD) function (Deng and Cai 2011, Yin *et al.* 2011) as

$$r(x) = \sum_{k=1}^{N} \sqrt{2\varphi(n_k)\Delta n}\cos(2\pi n_k x + \theta_k) \qquad (24)$$

where θ_k is the random phase angle uniformly distributed from 0 to 2π; $\varphi()$ is the PSD function (m³/cycle) for the road surface elevation; and n_k is the wave number (cycle/m). In

the present study, the following PSD function (Yin *et al.* 2011) has been used

$$\varphi(n) = \varphi(n_0)(\frac{n}{n_0})^{-2} \qquad (n_1 < n < n_2) \qquad (25)$$

where n is the spatial frequency (cycle/m); n_0 is the discontinuity frequency of $1/2\pi$ (cycle/m); $\varphi(n_0)$ is the roughness coefficient (m³/cycle) whose value is chosen depending on the road condition; and n_1 and n_2 are the lower and upper cut-off frequencies, respectively. The International Organization for Standardization (1995) has proposed a road roughness classification index from A (very good) to E (very poor) according to different values of $\varphi(n_0)$.

3. Numerical examples

3.1 Case one - a simple uniform single-span beam

In order to study the effect of the pavement on the bridge vibration and to verify the present method of the traffic-pavement-bridge system, a typical traffic-pavement-bridge model shown in Fig. 5 is studied.

Fig. 5 shows a simply-supported beam subjected to multiple moving-sprung-mass systems, which is similar to the model studied by Yang *et al.* (2004). The vehicle sprung mass M_v is supported on a dashpot-spring unit with the spring constant k_v and damping c_v. For illustration, the effects of the tire mass are neglected. The beam parameters are: Young's modules E=2.87 GPa, moment of inertia I=2.90 m⁴, mass per-unit-length m=2303 kg/m, and beam length L=25 m.

3.1.1 Mid-span dynamic displacement of beam

The mid-span displacements of the same beam were studied by Yang *et al.* (2004) and Yin *et al.* (2010) for the sprung mass with a speed v=100 km/h. Therefore, the same speed for the single vehicle was also used for comparison and the effect of the pavement on the mid-span displacements of the beam were plotted in Fig. 6. As can be seen, (1) if the pavement is included in the model (marked by Single vehicle in the present model), the responses obtained by the present model are reduced significantly; (2) if the median traffic flow is considered, the responses (marked by traffic flow in the present model) are increased largely compared to that for the single vehicle. Thus, the displacements at the mid-span generally increase with the increase of vehicle occupancies. Meanwhile, by comparing Figs. 6(a) to 6(d), if the effects of pavement and road
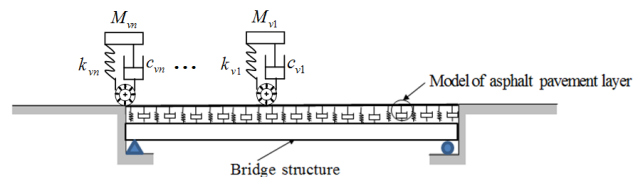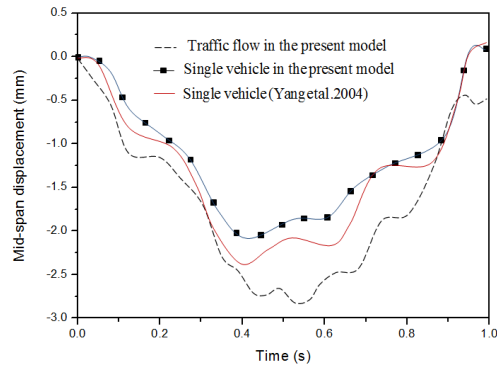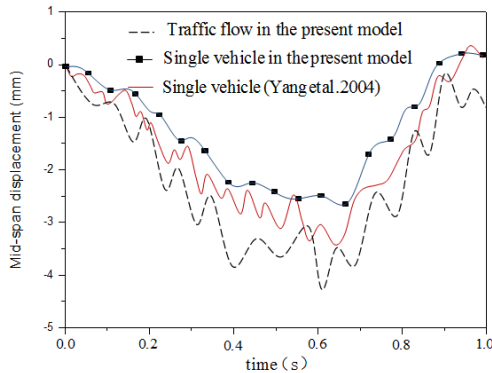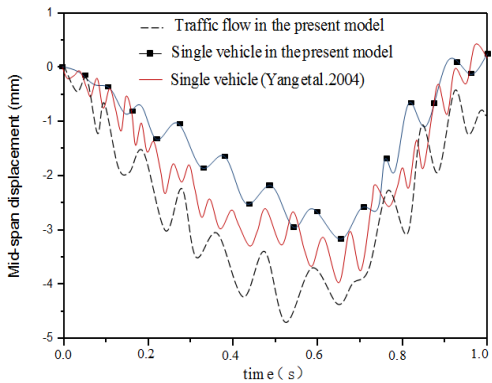

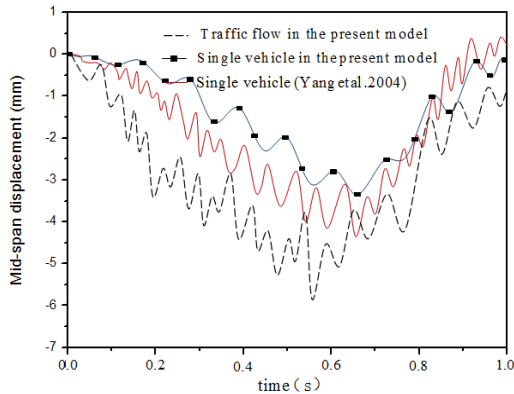Fig. 5 The simply supported beam model subjected to the moving vehicle

(a) Zero-roughness

(a) Zero-roughness

(b) Roughness=good

(b) Roughness=good

(c) Roughness=average

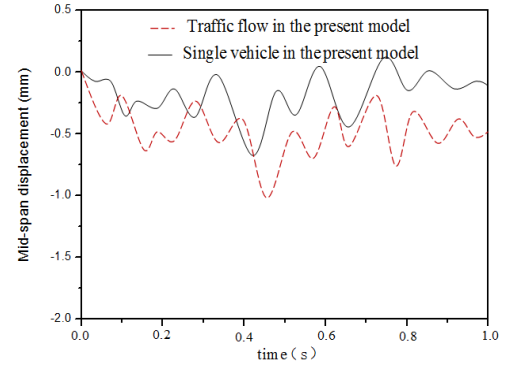(c) Roughness=average

(d) Roughness=poor
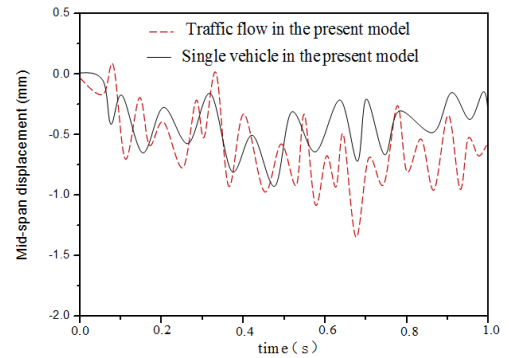
Fig. 6 Mid-span displacement of beam

(d) Roughness=poor
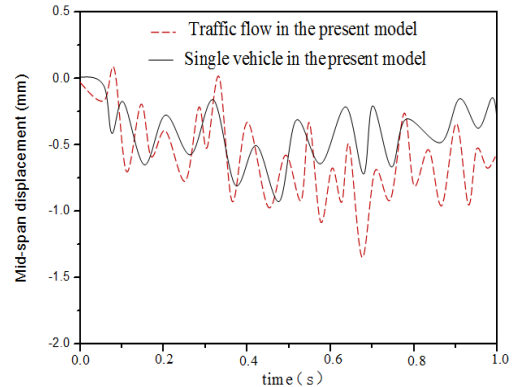
Fig. 7 Mid-span displacement of pavement

roughness are both considered, the effect of the pavement on the mid-span deflections are increased very significantly with the road surface classification increases.
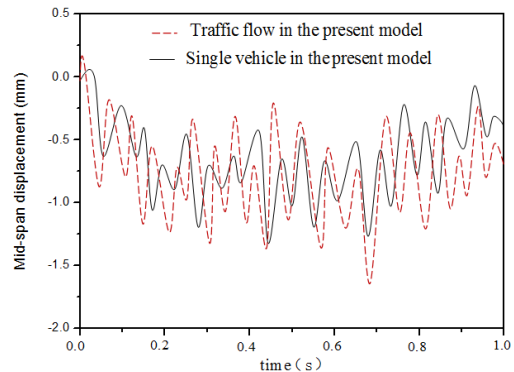
3.1.2 Mid-span dynamic displacement of pavement

In this study, using the present model of traffic-pavement-bridge coupled vibration system, the effect of traffic flow and road roughness on the pavement

displacements were studied and plotted in Fig. 7. By comparing Figs. 7(a) to 7(d), one observes that, if the effects of traffic flow and road roughness are both considered, the mid-span deflections of pavement are affected by the vehicular numbers in the traffic flow and also are increased very significantly with the road surface classification increases. Therefore, neglecting the effect of the pavement on bridge-vehicle coupled vibration may result in a conservative design.

3.2 Case two - a real suspension bridge

For long-span bridges such as suspension bridges, due to the small stiffness in the three dimensional directions, the vertical vibration of the long span bridge can easily be excited by traffic flows, and the vibration of bridge and pavement under stochastic traffic flows may be significant for the bridge and pavement designer (Chen and Wu 2010). As shown in Fig. 8, a suspension bridge was constructed in 2012, located in Sichuan Province, China. The geometrical characteristics of the bridge are: a total length of 1295.89 m, the longest span of 820 m, and a bridge width of 29.78 m.

3.2.1 Numerical model of the bridge

Based on the configuration of the bridge, a finite element (FE) model was created for this bridge, as shown in Fig. 9. Before being used in the numerical simulation, the FE bridge model was updated based on the results of a modal test by ambient vibration method. The details of the experimental setup and model updating are similar with that by Yin *et al*. (2011). Based on the configuration of the bridge, the bridge girders, tower, and railings were all modeled with solid elements. The main-cable and suspender were modeled with link elements, and a rigid connection was assumed between the main-cable and suspenders. A rigid connection was also assumed between both stiffening girder and diaphragms and between stiffening girder and bridge deck. In the study, the model of pavement was simulated using the Euler-Bernoulli beam supported on the Kelvin model, and the Kelvin model in the FE model was simulated using the equivalent method by solid element in Ansys software (shown in Fig. 9(b)).
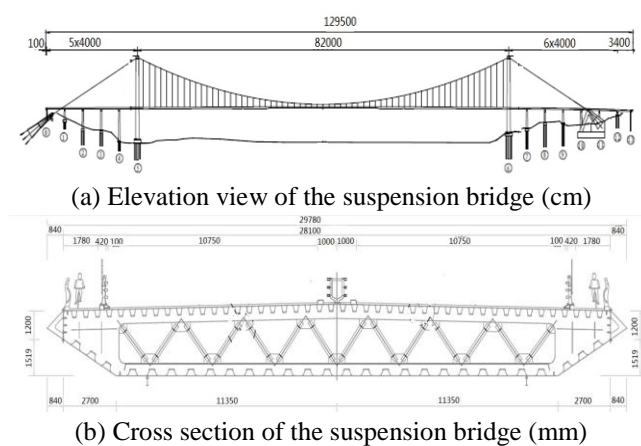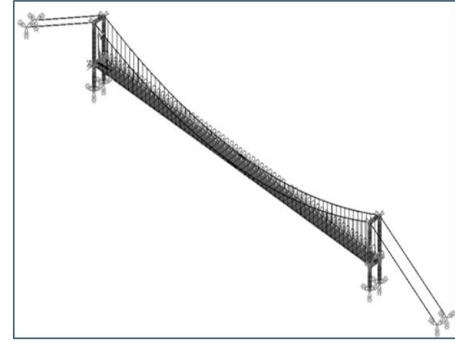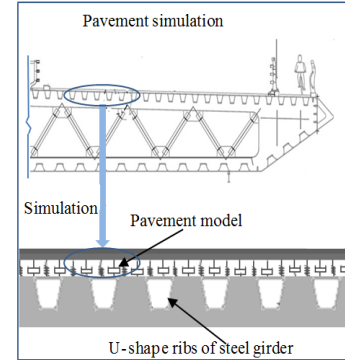

(a) FE Model of the bridge

(b) The schematic of deck pavement simulation

Fig. 9 The numerical model of the bridge

Table 2 The parameters of the 3-D vehicle

Truck Parameter	Value
Mass of truck body m_t	26745 kg
Pitching moment of inertia of truck body I_{zt}	172,160 kg.m^2
Rolling moment of inertia of truck body I_{xt}, I_{yt}	61,496 kg.m^2
Mass of truck front axle m_{a1}, m_{a2}	710kg
Mass of truck rear axle m_{a3}, m_{a4}	800kg
Suspension spring vertical stiffness of the first axle K_{sz}^1, K_{sz}^2	242604 (N/m)
Suspension spring longitudinal/lateral stiffness of the first axle K_{sy}^1, K_{sy}^2, K_{sx}^1, K_{sx}^2	102302 (N/m)
Suspension vertical damper of the first axle C_{sz}^1, C_{sz}^2	2190 (N.s/m)
Suspension longitudinal/lateral damper of the first axle C_{sy}^1, C_{sy}^2, C_{sx}^1, C_{sx}^2	1690(N.s/m)
Suspension spring vertical stiffness of the second axle K_{sz}^3, K_{sz}^4	1903172(N/m)
Suspension spring longitudinal/lateral stiffness of the second axle K_{sy}^3, K_{sy}^4, K_{sx}^3, K_{sx}^4	1003031(N/m)
Suspension vertical damper of the second axle C_{sz}^3, C_{sz}^4	7882(N.s/m)
Suspension longitudinal/lateral damper of the second axle C_{sy}^3, C_{sy}^4, C_{sx}^3, C_{sx}^4	5869(N.s/m)
Radial direction spring stiffness of the tire k_{ty}	276770 (N/m)
Radial direction spring damper coefficient of the tire c_{ty}	1990 (N.s/m)
Length of the patch contact	345 mm
Width of the patch contact	240 mm
Distance between the front and the center of the truck l_1	3.73 m
Distance between the rear axle and the center of the truck l_2	1.12 m
Distance between the right and left axles s_1	2.40 m

(a) Elevation view of the suspension bridge (cm)

(b) Cross section of the suspension bridge (mm)

Fig. 8 A suspension bridge

Table 3 The parameters of the single DOF vehicle model

Parameters	unit	Sedan car	Light truck
Sprung mass	kg	1611	4870
Stiffness of suspension system(K_{sx}^1, K_{sy}^1, K_{sz}^1)	N/m	434920	500000
Damping(C_{sx}^1, C_{sy}^1, C_{sz}^1)	N/(m/s)	5820	20000

3.2.2 The parameters of traffic vehicles

Both the 18 DOFs of 3-D vehicle dynamic model and the single DOF of vehicle model are used in the simulation. Mechanical and geometric properties are listed in Tables 2-3 and can be obtained from Yin *et al.* (2011) and Chen and Cai (2007).

3.2.3 The dynamic responses of the suspension bridge under two traffic flow occupancies

The Transportation Research Board classifies the "level of service" from a driving operation under a desirable condition to an operation under forced or breakdown conditions (Chen and Wu 2010). In following sections, two traffic flow occupancies, including the median traffic $\rho=0.15$ and busy traffic flow $\rho=0.3$, are used to study the dynamic responses of the bridge under the good classification of surface roughness. The dynamic responses of the bridge are shown in Figs. 10 and 11.

It is found from Fig. 10 that pavement plays a significant role on the vertical displacements. For example, when the vehicle occupancy is under median traffic, the maximal vertical displacements at mid-span (1/4 span) increase from 18.80 (20.43) cm to 26.0 (27.45) cm for two situations with and without considering the effects of pavement. Therefore, from this numerical example, the decreased degree of maximal vertical displacements by considering the pavement can be reached about 27.7% (25.6%). Meanwhile, the vertical displacements at the mid-span generally increase with vehicle occupancies. For example, when the effect of pavement is considered, the maximum vertical displacements at the mid-span (and 1/4 span) increase from 18.80 (20.43) cm to 25.09 (25.58) cm when the vehicle occupancy increases from the median traffic to the busy traffic.

Fig. 11 shows that if the effects of pavement and traffic flow are both considered, the mid-span deflections are increased very significantly with the road surface classification increases. When the effect of pavement is considered, the maximal vertical displacement at mid-span (1/4 span) increases from 18.80 (20.43) cm to 22.5 (22.1) cm for two road surface with good and poor classifications.

As discussed earlier, the dynamic responses of the pavement based on the vehicle-pavement-bridge coupled vibration system is significant. Using the present model of traffic-pavement-bridge coupled vibration system, the effect of traffic flow and road roughness on the pavement displacements were studied and plotted in Fig. 12. By comparing Figs. 12(a) to 12(b), one observes that, if the effects of traffic flow and road roughness are both considered, the mid-span deflections of pavement are affected by the vehicular numbers in the traffic flow and

also are increased very significantly with the road surface classification increases.
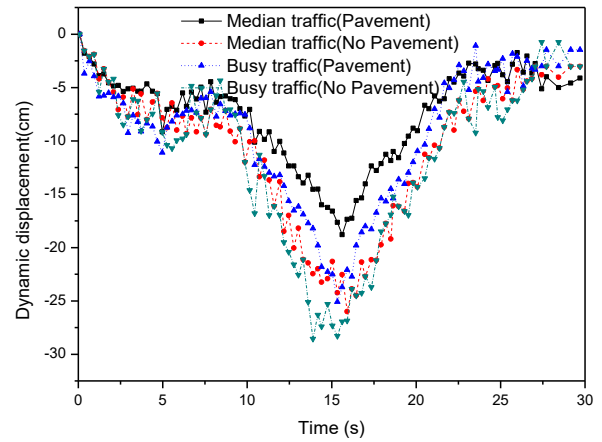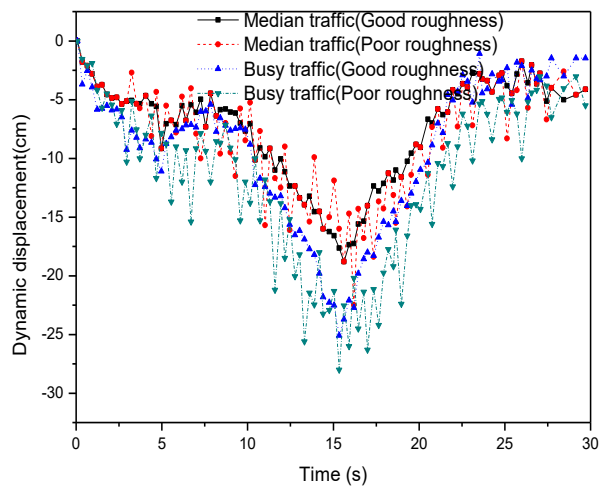

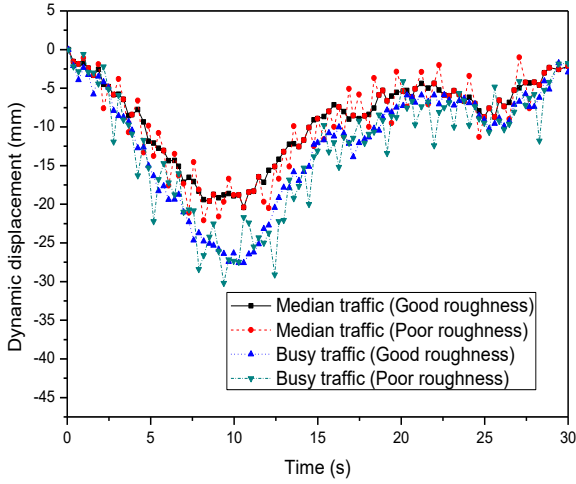(a) Vertical displacements of mid-span
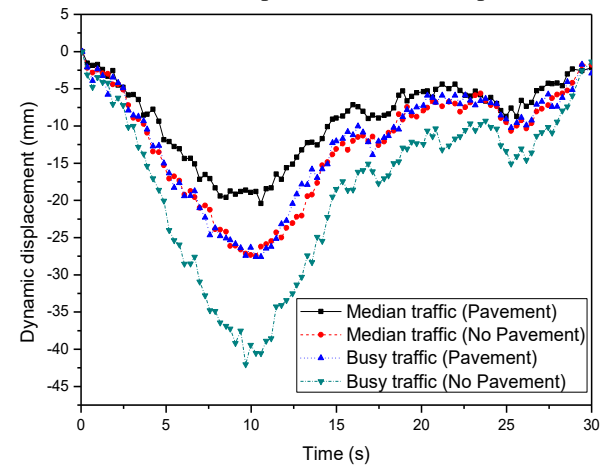
(b) Vertical displacements of 1/4 span

Fig. 10 The effect of pavement on the vertical displacement of stiffening girder
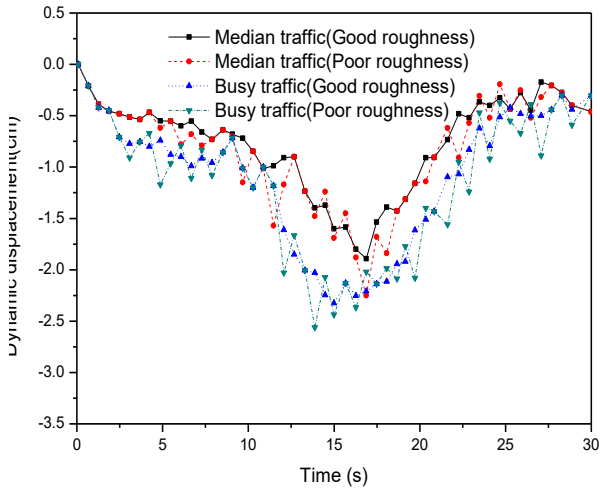

(a) Vertical displacements of mid-span

Fig. 11 The effect of road roughness on the vertical displacement of stiffening girder
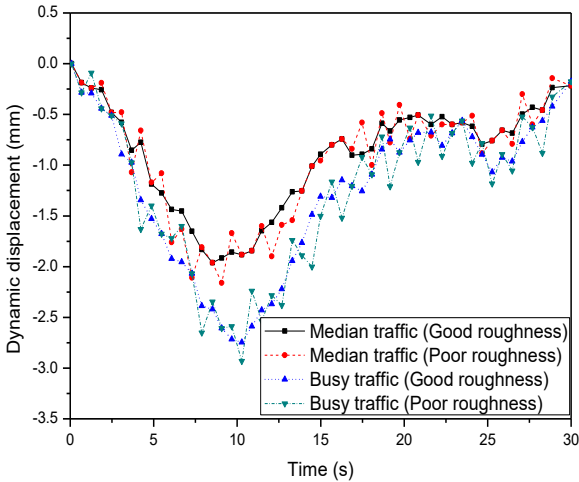
(b) Vertical displacements of 1/4 span

Fig. 11 Continued
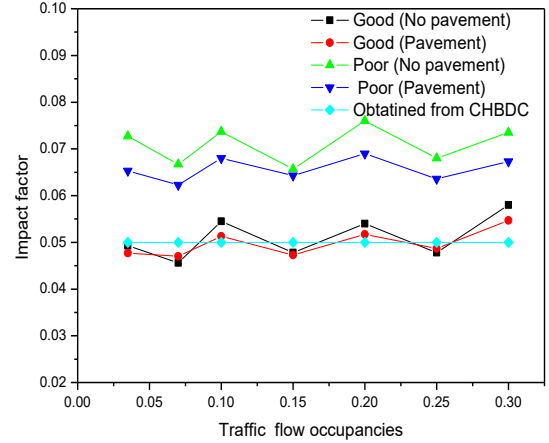
(a) Vertical displacements of mid-span
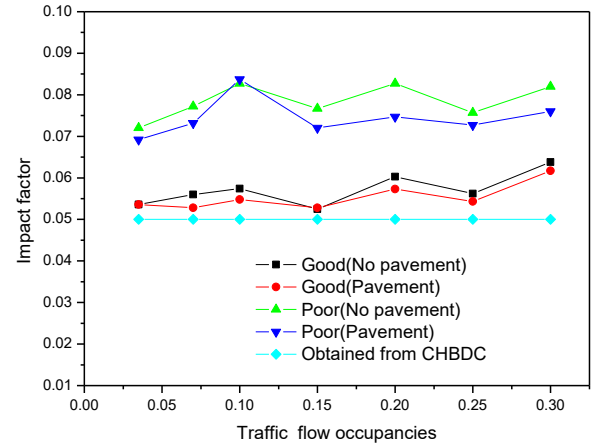
(b) Vertical displacements of 1/4 span

Fig. 12 The effect of road roughness on the vertical displacement of pavement

3.2.4 The comparison of impact factor under two traffic flow occupancies and road surface roughness

In the bridge design, the effects of moving vehicles on

(a) Mid-span

(b) 1/4 span

Fig. 13 Comparison of impact factor with the CHBDC and present method under road roughness

the vibration of bridge are usually defined by the impact factor. The impact factors in the design codes are not usually consider the effect of pavement, traffic flows, and road surface roughness. Therefore, more theoretical support was needed to study the impact for long-span suspension bridges. In this study, the impact factor is defined as follows

$$IM = \frac{R_d(x) - R_s(x)}{R_s(x)} \qquad (26)$$

where $R_d(x)$ and $R_s(x)$ are the maximum dynamic and static response of the bridge at location x, respectively.

To compare the impact factor obtained from design codes and the present method, the Chinese highway bridge design code (CHBDC) (2004) was given as an example, where the *IM* is defined as a function of the natural frequency of the bridge as shown below

$$\begin{cases} IM = 0.05, \ when \ f < 1.5 Hz; \\ IM = 0.1767 ln(f) - 0.0157, \ when \ 1.5 \ Hz \le f \le 14 Hz; \\ IM = 0.45, \ when \ f > 14 Hz \end{cases} \quad (27)$$

where *f* is the natural frequency of the bridge.

Fig. 13 shows the impact factors obtain by the CHBDC and present code under two classifications of road

roughness. It can be obtained that the impact factors obtained from CHBDC are both much smaller than the real values for two situations with and without effects of considering the pavement and under poor surface condition. For the situation of considering the pavement effect, the impact factor of 1/4 span can arrive at 0.083 when the road roughness deteriorated to poor classification. Meanwhile, without considering the pavement effect, the obtained impact factors are larger than those for the with considering pavement effect, which may be one of the main reasons that the calculated impact factors in the most studies are usually more larger than the measured impact factors. Thus, the effect of the pavement on impact factor cannot be neglected.

4. Conclusions

This study is mainly focused on establishing a new methodology considering fully the effects of bridge deck pavement, probabilistic traffic flows, and varied road roughness conditions. The bridge deck pavement was modeled as a Euler-Bernoulli beam supported on the Kelvin model; the typical traffic flows was simulated by the improved CA traffic flow model; two vehicle models, a eighteen DOFs vehicle model and a single vehicle model, were respectively used to simulate all vehicles in the traffic flow to be computationally efficient; and the traffic-pavement-bridge coupled equations were established by combining the equations of motion of both the vehicles, pavement, and bridge using the displacement and interaction force relationship at the contact locations. The numerical study shows that:

(1) The pavement plays a significant role on the vibration of vehicle-bridge coupled system. Based on the example in the paper, the decreased degree of maximal vertical displacements with pavement effects is about 27.7%;

(2) Using the present model of traffic-pavement-bridge coupled vibration system, the effect of traffic flow and road roughness on the pavement displacements can be investigated. The simulated results show that the mid-span deflections of pavement are affected by the vehicular numbers in the traffic flow and are increased very significantly with the road surface classification changing from good to poor.

(3) The impact factors obtained from CHBDC are much smaller than the real values for both situations with and without effects of pavement under the poor roughness conditions. For the situation of considering the pavement effect, the impact factor of 1/4 span can arrive at 0.083 when the road roughness deteriorated to poor classification. Meanwhile, by considering the pavement effect, the obtained impact factors are decreased significantly to the same magnitude level corresponding to those for the without considering pavement effect.

Acknowledgments

References

Andersen, L., Nielsen, S.R.K. and Kirkegaard, P.H. (2001), "Finite element modeling of infinite Euler beams on Kelvin foundations exposed to moving loads in converted coordinates", *J. Sound Vib.*, **241**(4), 587-604.

Cai, Y.Q., Chen, Y., Cao, Z.G., Sun, H.L. and Guo, L. (2015), "Dynamic responses of a saturated poroelastic half-space generated by a moving truck on the uneven pavement", *Soil Dyn. Earthq. Eng.*, **69**, 172-181.

Cao, Z.G., Cai, Y.Q., Sun, H.L. and Xu, C.J. (2011), "Dynamic responses of a poroelastic half-space from moving trains caused by vertical track irregularities", *Int. J. Numer. Anal. Methods Geomech.*, **35**(7), 761-786.

Chen, S.R. and Cai, C.S. (2007), "Equivalent wheel load approach for slender cable-stayed bridge fatigue assessment under vehicle and wind: feasibility study", *J. Bridge Eng.*, **12**(6), 755-764.

Chen, S.R. and Wu, J. (2010), "Dynamic performance simulation of long-span bridge under combined loads of stochastic vehicle and wind", *J. Bridge Eng.*, **15**(3), 219-230.

Chinese highway bridge code (2004), "Standard of the people's republic of china quality standard-JTG D60", China general code for design of highway bridges and culverts.

Deng, L. and Cai, C.S. (2010), "Development of dynamic impact factor for performance evaluation of existing multi-girder concrete bridges", *Eng. Struct.*, **32**(1), 21-31.

Deng, L. and Cai, C.S. (2011), "Identification of dynamic vehicular axle loads: Demonstration by a field study", *J. Vib. Control*, **17**(2), 183-195.

Fryba, L. (1974), "Response of a beam to a rolling mass in the presence of adhesion", *Acta Technica CSAV*, **19**(6), 673-687.

Green, M.F. and Cebon, D. (1997), "Dynamic interaction between heavy vehicles and highway bridges", *Comput. Struct.*, **62**(2), 253-264.

Heider, Y., Avci, O., Markert, B. and Ehlers, W. (2014), "The dynamic response of fluid-saturated porous materials with application to seismically induced soil liquefaction", *Soil Dyn. Earthq. Eng.*, **63**, 120-137.

International Organization for Standardization (ISO) (1995), "Mechanical vibration-road surface profiles-reporting of measured data", ISO 8068: (E), Geneva.

Kim, S.M. and McCullough, B.F. (2003) "Dynamic response of plate on viscous Winkler foundation to moving loads of varying amplitude", *Eng. Struct.*, **25**(9), 1179-1188.

Kong, X.J., Gao, Z.Y. and Li, K.P. (2006), "A two lane celluar automata model with influence of next nearest neighbor vehicle", *Commun. Theo. Phys.*, **45**(4), 657-662.

Kuo, C.M., Fu, C.R. and Chen, K.Y. (2011), "Effects of pavement roughness on rigid pavement stress", *J. Mech.*, **27**(1), 1-8.

Law, S.S. and Zhu, X.Q. (2005), "Bridge dynamic responses due to road surface roughness and braking of vehicle", *J. Sound Vib.*, **282**(3-5), 805-830.

Mamlouk, M.S. (1997), "General outlook of pavement and vehicle dynamics", *J. Transport Eng.*, **123**(6), 515-517.

Markow, M., Hedric J.K., Bradmeyer, B. and Abbo, E. (1988), "Analyzing the interaction between vehicle loads and highway pavements", *Proceeding of the 67th annual meeting, Transpotation Research Board*, Washington, D.C.

Nagel, K. and Schreckenberg, M. (1992), "A cellular automaton model for freeway traffic", *J. Phys. (France)*, **2**(12), 2221-2229.

Wang, T.L., Huang, D.Z. and Shahawy, M. (1992), "Dynamic response of multi-girder bridges", *J. Struct. Eng*., **118**(8), 2222-2238.

Yang, Y.B., Cheng, M.C. and Chang, K.C. (2013), "Frequency vibration in vehicle-bridge interaction systems", *J. Struct. Stabil. Dyn*. **13**(2), 1350019.

Yang, Y.B., Yau, J.D. and Wu, Y.S. (2004), "Vehicle-bridge interaction dynamics with applications to high-speed railways", World Scientific, Singapore, 45-56.

Yin, X.F., Cai, C.S., Fang, Z. and Deng, L. (2010), "Bridge vibration under vehicular loads-tire patch contact versus point contact", *Int. J. Struct. Stabil. Dyn*., **10**(3), 529-554.

Yin, X.F., Fang, Z. and Cai, C.S. (2011), "Lateral vibration of high-pier bridges under moving vehicular loads", *J. Bridge Eng*., **16**(3), 400-412.

Yin, X.F., Liu, Y., Guo, S.H., Zhang, W. and Cai, C.S. (2016), "Three-dimensional vibrations of a suspension bridge under stochastic traffic flows and road roughness", *Int. J. Struct. Stabil. Dyn*., doi: 10.1142/S0219455415500388.

Zhang, W. and Cai, C.S. (2012), "Fatigue reliability assessment for existing bridges considering vehicle speed and road surface conditions", *J. Bridge Eng*., **17**(3), 443-453.

Zhou, Y.F. and Chen, S.R. (2014), "Dynamic simulation of a long-span bridge-traffic system subjected to combined service and extreme loads", *J. Struct. Eng*., **141**(9), 04014215.

NM